J|A|C|S ARTICLES

Published on Web 11/02/2010

Resolving Rotational Motions of Nano-objects in Engineered Environments and Live Cells with Gold Nanorods and Differential Interference Contrast Microscopy

Gufeng Wang,[§] Wei Sun,[§] Yong Luo, and Ning Fang*

Ames Laboratory, U.S. Department of Energy, and Department of Chemistry, Iowa State University, Ames, Iowa 50011, United States

Received July 22, 2010; E-mail: nfang@iastate.edu

Abstract: Gold nanorods are excellent orientation probes due to their anisotropic optical properties. Their dynamic rotational motion in the 3D space can be disclosed with Nomarski-type differential interference contrast (DIC) microscopy. We demonstrate that by using the combination of gold nanorod probes and DIC microscopy, we are able to resolve rotational motions of nano-cargos transported by motor proteins at video rate not only on engineered surfaces but also on cytoskeleton tracks in live cells.

Introduction

Numerous biological nanomachines perform various functions that allow a creature to live and prosper. How these nanomachines work, especially in cellular environments, is poorly understood to date. Since the malfunction of any of these nanomachines will lead to severe disease(s), there is an imperative need for new techniques to investigate the composition, dynamics, and working mechanism of the nanomachines from the health and medicine sectors. In addition, these nanomachines show high power and energy efficiency. Therefore, there are always aspirations to let those bio-nanomachines step out of living organisms to find applications in nano-engineering.[1−3] This also requires a thorough understanding of these nanomachines.

Most of these nanomachines undergo motions that are essential to their functions. Understanding the characteristic translational and rotational motions is crucial to elucidate their working mechanisms. Translational motions can be revealed by a variety of single-molecule/particle tracking methods.[4−10] However, rotational motions in live cells are still largely unknown due to technical limitations. The current understanding of rotational motions at the single-molecule or single-nanoparticle level was acquired mostly from *in vitro* studies. The *in vitro* methods are based either on single-molecule fluorescence polarization[11−15] or on tracking translational movement of single-nanoparticle probes.[16−21] The fluorescence polarization-based methods are challenging for *in vivo* studies due to high autofluorescence background and high bleaching propensity of single fluorophores in the cellular environment. The particle tracking-based methods require specific geometries, e.g., fixed rotation center or axis, and thus are also not suitable for live-cell imaging.

Gold nanorods[22] show geometrically confined plasmon resonance modes: the longitudinal mode (along the long axis) and the transverse mode (along the short axis).[23] This results in anisotropic absorption and scattering properties of gold nanorods and thus allows their orientation to be determined with high precision in 2D.[24−26] Here, we show that by using

[§] These authors contributed equally to this work.

(1) Hess, H.; Bachand, G. D.; Vogel, V. *Chem.—Eur. J.* **2004**, *10*, 2110.
(2) van den Heuvel, M. G. L.; Dekker, C. *Science* **2007**, *317*, 333.
(3) Jia, L. L.; Moorjani, S. G.; Jackson, T. N.; Hancock, W. O. *Biomed. Microdevices* **2004**, *6*, 67.
(4) Saxton, M. J.; Jacobson, K. *Annu. Rev. Biophys. Biomater.* **1997**, *26*, 373.
(5) Kusumi, A.; Nakada, C.; Ritchie, K.; Murase, K.; Suzuki, K.; Murakoshi, H.; Kasai, R. S.; Kondo, J.; Fujiwara, T. *Annu. Rev. Biophys. Biomater.* **2005**, *34*, 351.
(6) Thompson, R. E.; Larson, D. R.; Webb, W. W. *Biophys. J.* **2002**, *82*, 2775.
(7) Katayama, Y.; Burkacky, O.; Meyer, M.; Brauchle, C.; Gratton, E.; Lamb, D. C. *ChemPhysChem* **2009**, *10*, 2458.
(8) Joo, C.; Balci, H.; Ishitsuka, Y.; Buranachai, C.; Ha, T. *Annu. Rev. Biochem.* **2008**, *77*, 51.
(9) Toprak, E.; Balci, H.; Blehm, B. H.; Selvin, P. R. *Nano Lett.* **2007**, *7*, 2043.
(10) Jaqaman, K.; Loerke, D.; Mettlen, M.; Kuwata, H.; Grinstein, S.; Schmid, S. L.; Danuser, G. *Nat. Methods* **2008**, *5*, 695.
(11) Sase, I.; Miyata, H.; Ishiwata, S.; Kinosita, K. *Proc. Natl. Acad. Sci. U.S.A.* **1997**, *94*, 5646.
(12) Forkey, J. N.; Quinlan, M. E.; Shaw, M. A.; Corrie, J. E. T.; Goldman, Y. E. *Nature* **2003**, *422*, 399.
(13) Toprak, E.; Enderlein, J.; Syed, S.; McKinney, S. A.; Petschek, R. G.; Ha, T.; Goldman, Y. E.; Selvin, P. R. *Proc. Natl. Acad. Sci. U.S.A.* **2006**, *103*, 6495.
(14) Xiao, L. H.; Qiao, Y. X.; He, Y.; Yeung, E. S. *Anal. Chem.* **2010**, *82*, 5268.
(15) Ha, T.; Laurence, T. A.; Chemla, D. S.; Weiss, S. *J. Phys. Chem. B* **1999**, *103*, 6839.
(16) Yasuda, R.; Noji, H.; Kinosita, K.; Yoshida, M. *Cell* **1998**, *93*, 1117.
(17) Itoh, H.; Takahashi, A.; Adachi, K.; Noji, H.; Yasuda, R.; Yoshida, M.; Kinosita, K. *Nature* **2004**, *427*, 465.
(18) Adachi, K.; Oiwa, K.; Nishizaka, T.; Furuike, S.; Noji, H.; Itoh, H.; Yoshida, M.; Kinosita, K. *Cell* **2007**, *130*, 309.
(19) Nitzsche, B.; Ruhnow, F.; Diez, S. *Nat. Nanotechnol.* **2008**, *3*, 552.
(20) Kukura, P.; Ewers, H.; Muller, C.; Renn, A.; Helenius, A.; Sandoghdar, V. *Nat. Methods* **2009**, *6*, 923.
(21) Yajima, J.; Mizutani, K.; Nishizaka, T. *Nat. Struct. Mol. Biol.* **2008**, *15*, 1119.
(22) Jana, N. R.; Gearheart, L.; Murphy, C. J. *J. Phys. Chem. B* **2001**, *105*, 4065.
(23) Gans, R. *Ann. Phys.—Berlin* **1915**, *47*, 270.
(24) Sonnichsen, C.; Alivisatos, A. P. *Nano Lett.* **2005**, *5*, 301.
(25) Spetzler, D.; York, J.; Daniel, D.; Fromme, R.; Lowry, D.; Frasch, W. *Biochemistry* **2006**, *45*, 3117.
(26) Chang, W. S.; Ha, J. W.; Slaughter, L. S.; Link, S. *Proc. Natl. Acad. Sci. U.S.A.* **2010**, *107*, 2781.

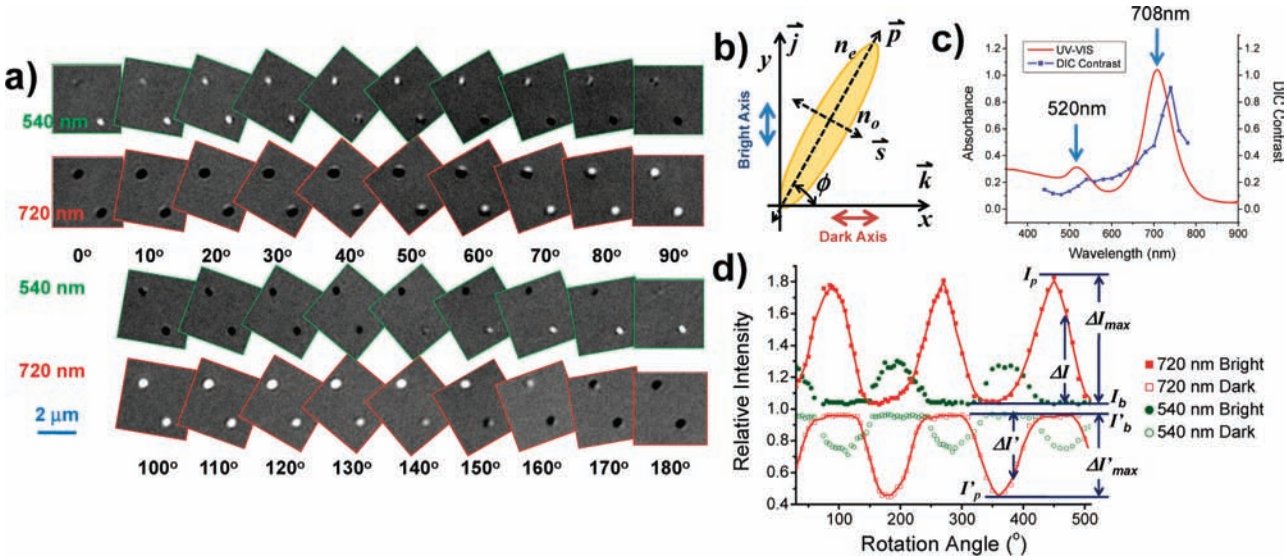

Figure 1. Gold nanorod orientations in 2D space. (a) DIC images of two 25 × 73 nm gold nanorods at different orientations in 2D space. The same nanorods were illuminated at their transverse (540 nm) or longitudinal plasmonic resonance wavelengths (720 nm). The gold nanorods were positively charged, physically adsorbed on a negatively charged glass slide, and submerged in deionized water. The glass slide was fixed on a rotating stage that allows 360° rotation. (b) Definition of the 2D orientation (*azimuth angle* ϕ) of a nanorod with respect to the polarization directions of the two illumination beams in a DIC microscope. Other symbols are explained in the Supporting Information. (c) UV−vis spectrum of the gold nanorod suspension in deionized water (red) and DIC spectrum of an immobilized, randomly orientated gold nanorod (blue). The DIC contrast is defined as the difference between the maximum and the minimum intensities divided by the average local background intensity. The two DIC peaks are red-shifted compared to their plasmon resonance wavelengths. (d) Periodic changes of the bright/dark intensities of a gold nanorod when rotated under a DIC microscope and illuminated at the two DIC peak wavelengths. All intensities are relative to the background level. The periodic patterns at these two illumination wavelengths are shifted by ~90°, consistent with the relative orientation between the transverse and longitudinal plasmonic resonance modes.

Nomarski-type differential interference contrast (DIC) microscopy,[27] which utilizes *two orthogonally polarized* illumination beams, the nanorod orientation can be resolved in both 2D and 3D in engineered environments and live cells.

Results and Discussion

2D and 3D Orientation of Gold Nanorods. Nomarski-type DIC microscopes are in principle two-beam interferometers. Each of the two orthogonally polarized illumination beams creates an *independent* intermediate image. One such image is shifted laterally by ~100 nm and then overlapped with the other to generate the final interference image. For *isotropic* samples, such as nanospheres, the two intermediate images are *identical*, thus leading to evenly distributed bright and dark intensities. For optically *anisotropic* samples, such as gold nanorods, the two intermediate images are different because the two illumination beams are phase-delayed to different extents, depending on the orientation of the nanorod relative to the two polarization directions. Therefore, the DIC images of gold nanorods appear as diffraction-limited spots with disproportionate bright and dark parts. Figure 1a shows the DIC images of two 25 × 73 nm gold nanorods positioned at different orientations and illuminated at their plasmon resonance wavelength: 540 nm for the transverse mode or 720 nm for the longitudinal mode (Figure 1c).

The orientation of a gold nanorod, i.e., the angle ϕ between the nanorod's long axis and the *x*-polarization direction as defined in Figure 1b, can be determined using the bright *or* dark intensities of its DIC images collected at 720 nm. The relative brightness $\Delta I/\Delta I_{max}$ (defined in Figure 1d) adopts a $\sin^4$ relationship with ϕ (for details, please see the Supporting Information):

$$\phi = a \sin(\Delta I/\Delta I_{max})^{1/4} \quad (1)$$

Similarly, the relative darkness $\Delta I'/\Delta I'_{max}$ adopts a $\cos^4$ relationship with ϕ:

$$\phi = a \cos(\Delta I'/\Delta I'_{max})^{1/4} \quad (2)$$

It is worthwhile to mention that the relative brightness and relative darkness are measures of effective projections of the nanorod onto the two polarization directions.

The errors of the angle determination are directly related to the precision of the DIC intensity measurement. For example, when the relative error of intensity measurement is ~0.5% (as in Figure 1d), the standard deviation of ϕ determined for a 25 × 73 nm gold nanorod is ~0.8°, that is, a 2−3° angular resolution in nearly the entire range. We also estimated the error of angle determination when these gold nanorods are used in live cells as orientation probes to track highly dynamic processes. For imaging live cells at video rates (32 frames/s) with an Andor EMCCD camera on a Nikon Eclipse 80i microscope, the relative error of intensity measurement under optimized conditions rises to ~1.5%, resulting in a standard deviation of the angle determination less than 3° (or an angular resolution of ~9°) for a 25 × 73 nm gold nanorod. (See Supporting Information for details of 2D angle determination.)

When a gold nanorod is arbitrarily positioned in the 3D space, its 3D orientation (the elevation angle ψ and the azimuth angle ϕ, as defined in Figure 2) can be resolved due to the two *independent* measurements of the bright and dark intensities in *each* DIC image. In practice, the accuracy of the nanorod orientation determination in 3D is directly related to the signal-to-noise ratio of the bright/dark intensities, which declines when the projection of the nanorod on either of the polarization directions approaches zero. (See Supporting Information for details of 3D angle determination.)

(27) Pluta, M. *Advanced Light Microscopy*; Elsevier Science Publishing Co. Inc.: New York, 1989; Vol. 2.

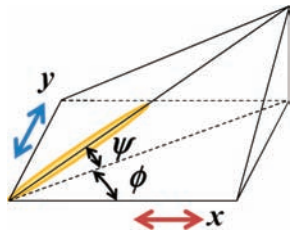

Figure 2. Definitions of the orientation angles of a nanorod in 3D space: the *elevation angle* ψ and the *azimuth angle* ϕ.

Rotational Motion of Gold Nanorods Attached on Gliding Microtubules. It is also possible to identify the nanorod rotational patterns from the dynamic rotation context. For example, when a nanorod rotates around a fixed axis, its orientations and the resulting DIC intensities must follow a characteristic pattern. A rotating nanorod goes through positions that can be resolved with either high or low confidence; thus, when the nanorod is followed continuously, the positions of low confidence can be resolved in the chronological context of the positions of high confidence, giving a better overall understanding of nanorod orientations in the time course.

Here we demonstrate that by using the combination of gold nanorod probes and DIC microscopy, we are able to resolve rotational motions of nano-cargos transported by motor proteins in 3D space. Motor proteins are essential to cellular functions by generating both translational and rotational motions, and they have shown great potential to serve as components of nanomachines to sort and shuttle cargos to designated locations in both engineered and biological environments.[28,29] One such example is shown in Movie 1 in the Supporting Information, where fluorescently tagged, reconstituted microtubules serving as carriers glide on kinesin-coated, microfabricated surface. Depending on the composition of the microtubules (number of protofilaments), the microtubule may rotate or not rotate around its longitudinal axis[30] when they are driven to move laterally. Apparently, such self-rotating motion is not readily resolved with conventional fluorescence microscopy. With carefully designed experiments and recently developed techniques, e.g., microtubules with a side arm,[30,31] quantum dot-assisted fluorescence interference contrast (FLIC) microscopy,[19] fluorescence microscopy with a wedged prism at the back focal plane of the objective,[21] etc., it becomes possible for researchers to detect the self-rotation of gliding microtubules. Until now, the majority of research reported was accomplished under ideal conditions, i.e., on clean, smooth surfaces. Here we show that by using the combination of gold nanorod probes and DIC microscopy, we are able to report rotational motions of nano-cargos during transport at video rate not only on *in vitro* engineered surfaces but also on cytoskeletons in live cells.

It is worth mentioning that small gold nanorods (10 × 35 nm) were used as reporters to track the self-rotation of gliding microtubules on flat substrates coated with full-length kinesin to avoid steric hindrance.[32] The observation wavelength was adjusted to 760 nm accordingly. By using a smaller probe, the signal strength was sacrificed, leading to lower signal-to-noise ratios. However, since the largest dimension of the gold nanorods is much smaller than the length of a full-length kinesin motor protein (~70 nm),[32] the continuous movement of the microtubule was not affected by the presence of the nanorod probe.

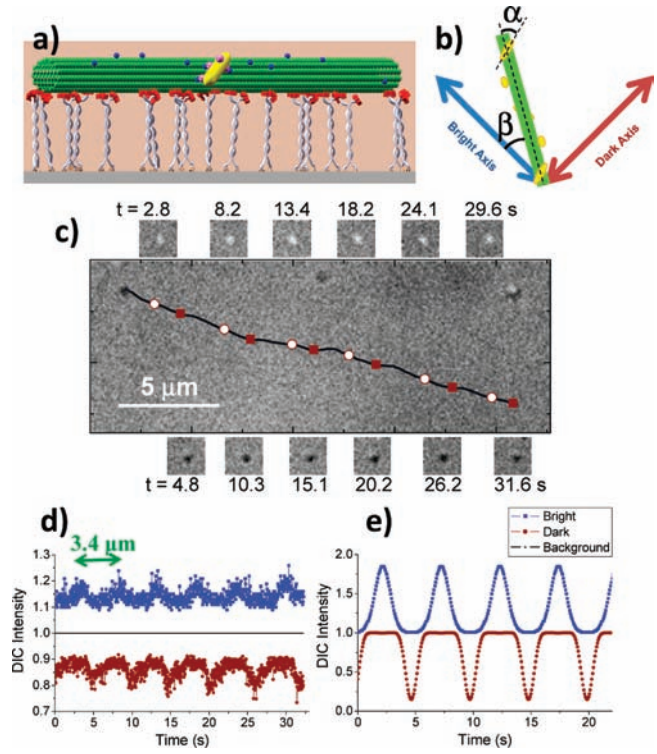

Figure 3. Cargo transport in engineered environments. (a) Scheme of a piece of gliding microtubule serving as the transport vehicle on a kinesin-coated glass slide. The 10 × 35 nm gold nanorod serves as the probe to detect the rotational motion of the microtubule. The blue dots are biotins, and the purple dots are neutravidins. (b) Definition of the microtubule *transport angle* β and the nanorod *binding angle* α. (c−e) Example of a gliding and self-rotating microtubule ($\beta \approx 151°$) as reported by the attached nanorod probe (Movie 2, Supporting Information): (c) trace and alternating bright-and-dark DIC images of the nanorod, (d) measured DIC intensities as a function of time, and (e) simulated DIC intensities as a function of time. The microtubule was assumed to be gliding with a transport angle β of 151° with a velocity of 0.68 μm/s. The nanorod binding angle α was assumed to be 45°. The simulated DIC intensity variation pattern is consistent with that from the experiment.

As mentioned earlier, the bright/dark DIC pattern of a gold nanorod is determined by the effective projections of the nanorod onto the two polarization directions of the two illumination beams. The two polarization directions are named the *bright axis* and the *dark axis* in the following discussion. When a nanorod is firmly bound to a non-13-protofilament microtubule through multiple strong biotin−neutravidin linkages, its rotation along with the microtubule on kinesin-coated substrate gives rise to periodic image patterns, which are dependent on the *transport angle* β between the microtubule advancement direction and the bright axis and the nanorod *binding angle* α between the microtubule and the long axis of the nanorod (Figure 3b). Judging from the DIC intensity changing patterns, the details of the microtubule rotation, e.g., the periodical length of protofilament helices, can be obtained. Figure 3c−e shows an example of a nanorod binding to a gliding and self-rotating microtubule on a kinesin-coated glass substrate. The nanorod was transported in a direction of ~151° to the bright axis (Figure 3c and Movie 2 in the Supporting Information). The nanorod

(28) Hess, H.; Matzke, C. M.; Doot, R. K.; Clemmens, J.; Bachand, G. D.; Bunker, B. C.; Vogel, V. *Nano Lett.* **2003**, *3*, 1651.
(29) van den Heuvel, M. G. L.; De Graaff, M. P.; Dekker, C. *Science* **2006**, *312*, 910.
(30) Ray, S.; Meyhofer, E.; Milligan, R. A.; Howard, J. *J. Cell Biol.* **1993**, *121*, 1083.
(31) Yajima, J.; Cross, R. A. *Nat. Chem. Biol.* **2005**, *1*, 338.
(32) Kerssemakers, J.; Howard, J.; Hess, H.; Diez, S. *Proc. Natl. Acad. Sci. U.S.A.* **2006**, *103*, 15812.

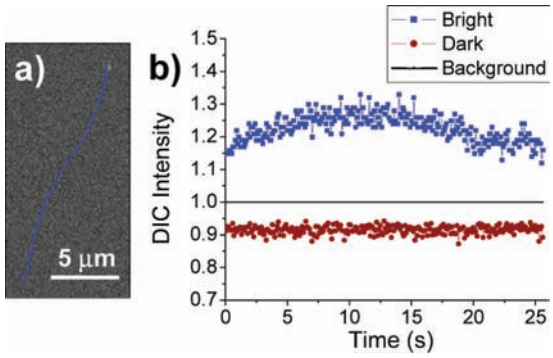

Figure 4. Example of a gliding and non-rotating microtubule ($\beta \approx 66°$) (Movie 3, Supporting Information): (a) trace of the nanorod and (b) measured DIC intensities as a function of time.

showed bright and dark images alternatingly (Figure 3c,d), indicating that the projections of the nanorod onto the two polarization axes change periodically as it rotated along with the self-rotating microtubule. The peak-to-peak distance is 3.4 μm, suggesting the microtubule is most likely composed of 12-protofilaments.[19,30]

We further simulated the DIC intensities of the nanorod as a function of time as it glides with a microtubule on the substrate with a transport angle β of 151° (Figure 3e). The gliding velocity was assumed to be 0.68 μm/s as in the experiment, and the nanorod binding angle α was assumed to be 45°. Since we focused on the DIC intensity variation profile and periodicity in the simulation, the DIC intensities ($\Delta I/\Delta I_{max}$ and $\Delta I'/\Delta I'_{max}$) of the nanorods were normalized to be between zero and unit. The simulated DIC intensity pattern is consistent with that from the experiment, showing that the periodical changing pattern is caused by the self-rotation of the gliding microtubule.

As a comparison, Figure 4 and Movie 3 in the Supporting Information show an example of a nanorod being transported by a non-rotating microtubule. The nanorod traveled a distance of ~15 μm along the direction of ~66° to the bright axis, showing slightly curved bright intensities and nearly constant, negligible dark intensities. The mostly bright image of the nanorod indicates that it binds to the microtubule at a very large angle (α close to 90°), yielding a large projection on the bright axis and a small projection on the dark axis. The situation that the nanorod binds in parallel to the microtubule axis (α close to 0°) thus can be excluded. In addition, the little variation in the DIC intensity indicates that the orientation of the nanorod did not change significantly over the whole period, and the microtubule was not rotating periodically over a distance of ~15 μm. Furthermore, we simulated the DIC intensity changing patterns with a microtubule transport angle $\beta = 67.5°$ at different nanorod binding angles α (Supporting Information, Supplementary Figure 4d). None of the simulated curves look similar to the experimental curves shown in Figure 4b, which further confirms that this is a non-rotating microtubule.

The DIC bright intensity does show a small curvature during the whole transport period, which is correlated with the curvature of the trace. The microtubule walked a backward "S" shape (Figure 4a). For a nanorod binding to the microtubule with a large angle (a large α), it will have relatively smaller projections on the bright axis at the two ends and a larger projection in the middle of the trace (see Supporting Information, Supplementary Figure 5). The corresponding DIC intensity will display lower bright intensities at the two ends and higher intensity in the middle, consistent with the experimental data. This shows that

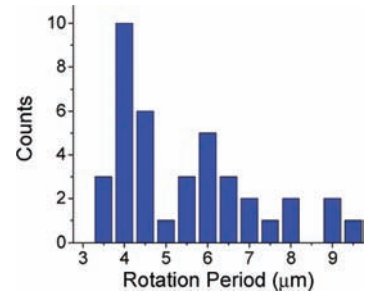

Figure 5. Statistics of the rotation period of gliding microtubules probed with 10 × 35 nm gold nanorods. A total of 98 cases were recorded and analyzed. Among them, 39 cases show clear periodic patterns, and the distribution of their rotation periods is plotted.

the variation of the DIC intensities is caused by the microtubule advancing direction rather than the self-rotation.

To assess the dependence of DIC intensity changing patterns on the transport angle β and the nanorod binding angle α, the DIC intensity changing patterns for different transport situations were simulated and plotted in Supplementary Figure 4 in the Supporting Information. We noticed that when the nanorod is parallel to the microtubule ($\alpha = 0$), the nanorod will not report the self-rotation of the microtubule at any transport angle. However, when α is larger than 10°, we shall see the periodic DIC intensity changing pattern at most of the transport directions. This means that when using gold nanorods as reporters, we will miss ~11% of the rotating cases, given that the nanorod has no preferred orientation when binding to the microtubule. In our experiments, we followed a procedure that favors the formation of 12-protofilament microtubules.[19] A total number of 98 cases were recorded and analyzed. Among them, 39 cases show clear periodic patterns, and the distribution of rotation period is plotted in Figure 5.

It also should be cautioned that, in order for gold nanorods to be a reliable rotation probe, they must be bound to the target firmly through multi-valent bonds. In this study, in order to achieve a multi-point attachment of the nanorod to the microtubule, we purposely increased the fraction of the biotin-labeled tubulins during the microtubule polymerization process. Still, we observed occasionally that nanorods showed irregular rotational motions during the gliding, possibly due to single-point attachment of the nanorod to the microtubule. Movie 4 in the Supporting Information shows such a case, where two nanorods bound to one microtubule. One nanorod gave nearly constant DIC contrast, indicating the microtubule was not rotating. The other nanorod yielded flickering images throughout, suggesting that it was rotating rapidly and randomly, possible due to a single-point attachment to the microtubule. These non-stable binding cases were excluded from the statistical analysis in Figure 5.

Rotational Motion of Gold Nanorods Being Transported in Live Cells. We further show that gold nanorod probes can disclose the rotational motions of nanorod-containing vesicles as they were being pulled on cytoskeleton tracks in live cells. TAT-modified gold nanorods with a dimension of 25 × 73 nm were naturally internalized by A549 human lung cancer cells, and their subsequent transport on cytoskeleton tracks was followed with DIC microscopy with an observation wavelength of 720 nm. The large gold nanorods (25 × 73 nm) were used to improve the signal-to-noise ratio in the complex cellular environment. Movie 5 in the Supporting Information shows a selected transport event where a nanorod-containing vesicle

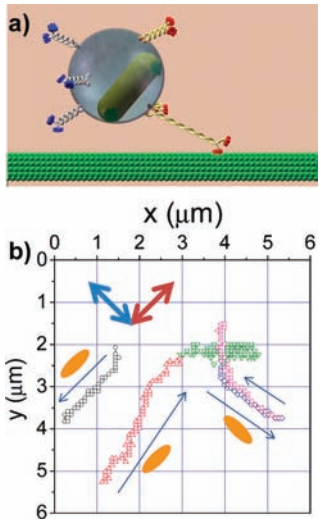

Figure 6. Cargo transport in live cells (Movie 5, Supporting Information). (a) Schematics of the intracellular microtubule transport of a gold nanorod-containing vesicle. The red and blue motor proteins represent kinesins and dyneins, respectively. (b) Traces and presumed orientations of the gold nanorod during the transport.

traveled a long distance (>6 μm) on multiple tracks toward different directions. The relatively fast transport velocity (average velocity 1.2 μm/s) suggests that the nanorod-containing vesicle was most likely transported on the microtubule tracks.[33] The nanorod gave nearly constant bright/dark intensities in the time course when being transported linearly. More interestingly, when the nanorod's moving direction changed ~90°, the DIC intensity pattern changed from completely dark to completely bright, indicating a ~90° turn in the focal plane also for the cargo's orientation. These observations suggest that the orientation of the cargo relative to the microtubule tracks is tightly controlled, resulting in a conveyor-like movement of vesicles on the microtubule network. Figure 6b shows the traces of the nanorod and the presumed orientation of the nanorod in Movie 5.

It is assumed that the nanorod is stationary with respect to the vesicle. There are several reasons that this assumption is valid. Endocytic vesicles are usually several tens of nanometers in diameter.[34] Considering the size of the nanorod (25 × 73 nm) and multiple assisting proteins and receptors, there is little room for the nanorod to diffuse randomly. More importantly, we observed that the nanorod showed a fixed orientation during the transport, indicating that the nanorod cannot experience active random rotational diffusion relative to the vesicle. Thus, we are observing the rotational motions of the vesicle during a transport process rather than the random motions of the nanorod inside the vesicle.

Movie 5 shows for the first time the dynamic orientation information of nano-objects in live-cell transport processes. The new approach may shed new light on many live-cell transport mysteries, such as the question whether molecular motors with different directionalities work in coordination or fight a "tug of war" to reverse the transport direction.[35−38]

Conclusions

We demonstrated that by using gold nanorod probes and DIC microscopy, rotational motions of nano-objects can be resolved at video rates in both engineered environments and live cells. Compared to single-molecule fluorescence polarization imaging, this method is more robust in terms of resistance to photobleaching and background noise. In our vision, this technique has great potential to investigate the working mechanisms of nanomachines by revealing their dynamic rotational motions in both micro- and nano-engineered structures and in live cells.

Experimental Section

DIC/Fluorescence Microscope. An upright Nikon Eclipse 80i microscope equipped with a heating stage was used in this study. This microscope can be switched between DIC mode and fluorescence mode. When the microscope was operated in DIC mode, a set of two Nomarski prisms, two polarizers, and a quarter-wave plate were installed. The samples were illuminated through an oil immersion condenser (numerical aperture 1.40), and the optical signals were collected with a 100× Plan Apo/1.40 oil immersion objective. In collecting DIC intensity spectra, a set of 25 filters with central wavelengths in the range of 400−780 nm and a full width at half-maximum (fwhm) of 10 nm was used. The optical filters were obtained from Thorlabs (Newton, NJ) or Semrock (Rochester, NY). The DIC images at a selected wavelength were collected by inserting the corresponding bandpass filter into the light path in the microscope. An Andor iXon^{EM}+ camera or a Photometrics Evolve camera (512 × 512 imaging array, 16 × 16 μm pixel size) was used to record the dynamic *in vivo* and *in vitro* transport at 32 frames/s. A Photometrics CoolSnap ES CCD camera (1392 × 1040 imaging array, 6.45 × 6.45-μm pixel size) was used to image immobilized gold nanorods in detail. When the Nikon microscope was operated in epi-fluorescence mode, samples were excited with a mercury lamp with proper bandpath filters applied in the excitation and emission channels. A rotary motor from Sigma Koki (model no. SGSP-60YAM) was coupled to the microscope stage to control the *z*-position of the sample. The CCD camera and the stage were synchronized by a homemade C++ computer program. MATLAB and NIH ImageJ were used to analyze the collected images and videos.

Preparation of Surface-Modified Gold Nanorods for Cell Experiments. Neutravidin-modified gold nanorods (10 × 35 nm) were purchased directly from Nanopartz (Salt Lake City, UT). TAT-coated gold nanorods were modified from cetyl trimethylammonium bromide (CTAB)-capped (25 × 73 nm, 1.3 × 10^{11} particles/mL, Nanopartz) gold nanorods. The size distribution and geometric profile were evaluated with transmission electron microscopy (Supporting Information, Supplementary Figure 1a) and agreed well with the manufacturer's data. The absorption spectrum of the particles in bulk solution (Figure 1b) was measured with a Cary 300 UV−vis spectrophotometer (Varian, Palo Alto, CA). To functionalize the surface of CTAB-coated gold nanorods with TAT 47−57 peptide (sequence: YGRKKRRQRRR; AnaSpec, San Jose, CA), a NHS-PEG disulfide linker (Sigma-Aldrich) was used by following a published protocol.[39] The NHS-PEG disulfide linker has both disulfide and succinimidyl functionalities for respective

(33) Lakadamyali, M.; Rust, M. J.; Zhuang, X. W. *Cell* **2006**, *124*, 997.
(34) Conner, S. D.; Schmid, S. L. *Nature* **2003**, *422*, 37.
(35) Kural, C.; Kim, H.; Syed, S.; Goshima, G.; Gelfand, V. I.; Selvin, P. R. *Science* **2005**, *308*, 1469.
(36) Gross, S. P.; Welte, M. A.; Block, S. M.; Wieschaus, E. F. *J. Cell Biol.* **2002**, *156*, 715.
(37) Muller, M. J. I.; Klumpp, S.; Lipowsky, R. *Proc. Natl. Acad. Sci. U.S.A.* **2008**, *105*, 4609.
(38) Gennerich, A.; Vale, R. D. *Curr. Opin. Cell Biol.* **2009**, *21*, 59.
(39) Narayanan, R.; Lipert, R. J.; Porter, M. D. *Anal. Chem.* **2008**, *80*, 2265.

chemisorption onto gold and facile covalent coupling of TAT peptide. Briefly, excessive surfactant was first removed from 1.0 mL of gold nanorod solution by centrifugation at 3000*g* for 10 min, and the particles were resuspended in 1.0 mL of 2 mM borate buffer. A proper amount of fresh NHS-PEG disulfide solution (in dimethyl sulfoxide) was added to reach a final thiol concentration of 0.2 mM and reacted with gold nanorods for 2 h. The solution was then cleaned by centrifugation and resuspended in 2 mM borate buffer. For TAT-modified gold nanorods, 2.0 μg of TAT peptide was added to the gold colloidal solution and reacted for 8 h. The gold nanorods were then blocked by adding 100 mL of 10% BSA solution (2 mM borate buffer) for over 8 h. Before use, the colloidal gold nanorod probes were cleaned by centrifugation and resuspended in 500 μL of 1% BSA (2 mM borate buffer). The concentrated gold colloidal solution was diluted in cell culture medium to a final concentration of 4.3×10^9 particles/mL for incubation with cells.

Imaging of Immobilized Gold Nanorods. The purchased gold nanorod solution was cleaned, diluted with 18.2-MΩ pure water to a proper concentration, and sonicated for 15 min at room temperature. Six microliters of the diluted solution was added onto a freshly cleaned glass slide and covered with a 22 × 22 mm No. 1.5 coverslip (Corning, NY). The positively charged gold nanorods were immobilized on the negatively charged surface of the glass slide by electrostatic forces. The glass slide was then placed on a 360° rotating mirror holder affixed onto the microscope stage. By rotating the mirror holder 5° or 10° per step, the nanorods were positioned in different orientations, and their DIC images at 540 or 720 nm were taken with the Photometrics CoolSnap ES CCD camera. The exposure time was adjusted to maintain the same background intensity at different wavelengths.

Full-Length Kinesin Motor Proteins. BL21 (DE3) *Escherichia coli* bacteria with the full-length His-tagged kinesin plasmid were kindly provided to us by Dr. Will Hancock from The Pennsylvania State University. The *E. coli* bacteria were induced to express kinesin with isopropyl β-D-1-thiogalactopyranoside (IPTG), and the kinesin was purified on a Ni column according to a published protocol.[40]

Preparation of Microtubule. All the tubulin proteins, GTP, and Taxol were purchased from Cytoskeleton (Denver, CO). Tubulin proteins were mixed and aliquoted in the following ratios: 86% unlabeled tubulin, 7% Rhodamine-labeled tubulin, and 7% biotinylated tubulin. Microtubules with 12-protofilaments were prepared according to published protocols:[41,42] 10 μL of BRB80 buffer supplemented with 9 μM tubulin, 4 mM $MgCl_2$, 0.5 mM GTP, and 10 μM Taxol was incubated at 37 °C for 3 h; microtubules were then diluted and stabilized in 100 μL of BRB80 buffer supplemented by 10 μM Taxol. Before the microtubules were introduced into the chamber for gliding assay, the microtubule solution was pipetted up and down to shorten the microtubules to the proper length.

***In Vitro* Transport.** Two strips of double-sided tape were put on a clean glass slide to serve as the spacers, and one clean coverslip was placed on top to form a chamber. BRB80 solution containing 0.5 mg/mL casein (Sigma, St. Louis, MO) was flowed into the chamber, and the chamber was kept at room temperature for 5 min. BRB80 solution containing 0.2 mg/mL casein, 0.2 mM MgATP, and kinesin was then introduced into the chamber to replace the previous liquid. After 5 min, BRB80 solution containing 0.2 mg/mL casein, 0.2 mM MgATP, 10 μM Taxol, and microtubules was introduced into the chamber and kept at room temperature for 5 min. Next, BRB80 solution containing 0.2 mg/mL casein, 0.2 mM MgATP, 10 μM Taxol, and neutravidin-modified gold nanorods (10 × 35 nm, Nanopartz, Salt Lake City, UT) was flowed into the chamber and kept at room temperature for 7 min. Finally, the chamber was filled with BRB80 solution containing 0.2 mg/mL casein, 1 mM MgATP, and 10 μM Taxol with an oxygen-scavenging system [50 μg/mL glucose oxidase (Sigma), 4 μg/mL catalase (Sigma), 1% (w/v) glucose (Sigma), and 0.1% (v/v) β-mercaptoethanol (Fluka)]. After each step, the chamber was washed twice with BRB80 solution containing 0.2 mg/mL casein and 0.2 mM MgATP. The sample slide was then observed under a DIC microscope.

Cell Culture and Intracellular Transport of Gold Nanorods. A549 human lung cancer cell line was purchased from American Type Culture Collection (CCL-185, ATCC, Manassas, VA). The cells were plated in a T25 cell culture flask (Corning) and grown in cell culture medium supplemented with 10% fetal bovine serum (FBS) in a cell culture incubator (37 °C, 5% CO_2). When subculturing, 150 μL of cell suspension solution was transferred to a 22 × 22 mm poly-L-lysine (PLL)-coated coverslip, housed in a 35-mm Petri dish (Corning). The Petri dish was left in the incubator for 1 h to let the cells attach to the coverslip. After 1.5 mL of the cell culture medium with 10% FBS supplement was added to immerse the coverslip, the Petri dish was left again in the incubator for 24 h. Gold nanorods were diluted in cell culture medium to the proper concentration and incubated with cells from 1 to 8 h as desired. The coverslip with cells was then put on a glass slide with two strips of double-sided tape as spacers to form a chamber and was put under a microscope for observation.

Simulation of DIC Intensity Changing Pattern of a Nanorod during Rotation. To validate the interpretation from the experimental DIC intensity traces, we used computer simulation to illustrate the theoretical DIC intensity changing patterns as the nanorod rotates in the 3D space. The relative DIC intensities of the bright part, $\Delta I/\Delta I_{max}$, and the dark part, $\Delta I'/\Delta I'_{max}$, were calculated using eqs A33 and A34 in the Supporting Information. In the simulation (Figures 3e and 4), the phase delay δ_1 was set to 90°, and δ_2 was set to 0° for simplicity. Since we are focusing on the DIC intensity variation profile and periodicity, the maximum DIC intensities ($\Delta I/\Delta I_{max}$ and $\Delta I'/\Delta I'_{max}$) of the nanorods were normalized to be between zero and unit in all cases.

Acknowledgment. The Ames Laboratory is operated for the U.S. Department of Energy by Iowa State University under contract no. DE-AC02-07CH11358. This work was supported by the Chemical Sciences, Geosciences, and Biosciences Division, Basic Energy Sciences, Office of Science, U.S. Department of Energy, and the Iowa Center for Advanced Neurotoxicology (Seed Funding). The authors thank Dr. William O. Hancock at The Pennsylvania State University for kindly providing BL21 (DE3) *E. coli* bacteria with the full-length His-tagged kinesin plasmid and Drs. Edward W. Yu and Feng Long at Iowa State University for help in purifying kinesin proteins.

Supporting Information Available: Theoretical section, supplementary figures, and five movies. This material is available free of charge via the Internet at http://pubs.acs.org.

JA106506K

(40) Hancock, W. O.; Howard, J. *J. Cell Biol.* **1998**, *140*, 1395.
(41) Ray, S.; Meyhofer, E.; Milligan, R. A.; Howard, J. *J. Cell Biol.* **1993**, *121*, 1083.
(42) Nitzsche, B.; Ruhnow, F.; Diez, S. *Nat. Nanotechnol.* **2008**, *3*, 552.